



## Improving Lung Region Segmentation Based on Lazy Snapping and Clustering for Aiding COVID-19 Diagnosis

Raihana Nur Safina Rahmad<sup>1</sup>, Aimi Salihah Abdul Nasir<sup>2,\*</sup>, Ooi Wei Heng<sup>1</sup>, Afifah Shuhada Rosmi<sup>1</sup>

<sup>1</sup> Faculty of Electrical Engineering and Technology, Universiti Malaysia Perlis, 02600 Arau, Perlis, Malaysia

<sup>2</sup> Sport Engineering Research Centre, Universiti Malaysia Perlis, 02600 Arau, Perlis, Malaysia

### ARTICLE INFO

#### Article history:

Received 30 March 2024

Received in revised form 20 September 2024

Accepted 7 October 2024

Available online 20 December 2024

#### Keywords:

Covid-19; Chest x-ray; Lung segmentation; Lazy snapping; Clustering algorithms

### ABSTRACT

The COVID-19 global pandemic, brought on by the rapid spread of the new coronavirus (SARS-CoV-2), has developed into one of the healthcare industry's most significant challenges in recent memory. Early detection of positive patients is essential to prevent the further spread of the COVID-19 virus. Chest x-ray (CXR) images of patients reporting shortness of breath initially led clinicians to suspect the presence of this novel virus. On CXR images, among the alterations detected in the lungs are indications of cloud region, also known as Ground-Glass Opacity. Consequently, the primary objective of this study is to develop a robust segmentation and to acquire an accurate segmented lung region in a CXR image, as this is a necessary step for accurate diagnosis using computer-aided diagnostic systems (CADs). The proposed methodology employs a multi-level segmentation strategy to improve the performance of lung region segmentation, where Lazy Snapping is utilized as pre-segmentation step to automatically remove the bone of the chest area, followed by clustering to achieve the complete segmentation. Furthermore, the advantage of fast *k*-means (FKM) clustering has also been utilized to obtain the desired lung region. The proposed strategy using Lazy Snapping and FKM was experimented on 150 CXR images and has achieved an average accuracy, sensitivity of and specificity of 92.38%, 85.23% and 96.27%, respectively. Based on the results obtained, this approach demonstrated efficacy in lung segmentation in chest x-ray images and has a significant potential for clinical use.

## 1. Introduction

The first incidence of COVID-19 in Wuhan was identified in December 2019. As of April 8, 2022, there were 494,587,638 confirmed cases of COVID-19 and 617,0283 reported deaths worldwide. Malaysia reported to the WHO 4,292,585 confirmed cases of COVID-19 from 3 January 2020 to 20 April 2022, with 35,228 fatalities. It is vital to diagnose positive cases as soon as possible to prevent the COVID-19 virus from spreading further around the world. Additionally, to those who are susceptible to infection and weak. Medical professionals began to suspect that people with shortness

\* Corresponding author.

E-mail address: [aimisalihah@unimap.edu.my](mailto:aimisalihah@unimap.edu.my)

<https://doi.org/10.37934/araset.54.1.138153>

of breath who had chest X-rays (CXR) might have this unique virus as soon as the illness was discovered. Anomalies in the lungs include evidence of the cloud region known as Ground-Glass Opacity (GGO) on CXR imaging. CXR, however, has several drawbacks. The difficulty in manually analysing CXR images is the issue. Because the cloud region creation in COVID-19 images and pneumonia appears to be similar, radiologists have trouble producing CXR images for patients with both conditions. Therefore, numerous studies have been conducted to aid medical professionals in diagnosing COVID-19 disease and pneumonia more accurately so that patients who are infected can receive thorough and prompt treatment [1-3].

Imaging techniques for the diagnosis of heart illness, such as CT angiography, echocardiography, and heart MRI, have advanced significantly during the previous 25 to 30 years. The initial imaging examination, however, was carried out using a chest x-ray for individuals with heart disease. It is simple for radiologists to use and is now widely available. A chest X-ray makes it relatively simple to monitor heart disease patients and, in some circumstances, to determine the disease's severity [4]. The diagnosis of COVID-19 is greatly aided by chest X-rays (CXR) and the assessment of the extent of lung damage caused by the virus regarding the practical advantages and widespread availability. The focus of this research was to use in-depth learning-based methods to automate the classification of COVID-19 from common and viral pneumonia on CXR based on the GGO.

In patients with COVID-19 disease and pneumonia disease, the characteristic radiographic uses chest CT scan and Chest X-Ray to obtain. Chest X-rays can also be used to monitor patients that have COVID-19 and pneumonia [5]. Compared to a chest X-ray, a chest CT scan provides a more detailed and accurate view of the chest, revealing the exact location and type of abnormality in a 3D image. While an X-ray gives a 2D image of solid tissues, CT scans capture bones, soft tissues, and blood arteries simultaneously. X-ray equipment is simpler and smaller than CT scanners, which rotate around the patient. A chest X-ray is an inexpensive first-look exam, but a chest CT scan may be necessary for a clearer image to proceed with diagnosis and treatment [4].

Image segmentation is a technique that divides a digital image into smaller groups, called segments, to simplify analysis. Labels are assigned to pixels, with each category having a unique name. Segmentation reduces complexity and speeds up object detection by feeding only a portion of the image into the detector. Two approaches to image segmentation are similarity and discontinuity. It is critical and urgent to develop automatic methods for medical image segmentation. Researchers have therefore made numerous attempts over the past few decades to propose diverse methodologies for medical image segmentation. Consequently, numerous research has been suggested. Elaziz *et al.*, [6] method approach uses the generalized extreme value (GEV) distribution to improve the density peaks clustering (DPC). The proposed model is validated on twelve COVID-19 CT images. It was compared to traditional k-means and DPC techniques as well, and it outperformed them on a number of criteria like PSNR, SSIM, and Entropy. As the result, suggested method reached 89% of SSIM while the DPC and K-means only reached 82% and 76% of SSIM in 11 out of 12 images, respectively.

In the 2021 study by Dixit *et al.*, a classifier that merges Differential Evolution (DE) with Particle Swarm Optimization (PSO), incorporates KM clustering as its segmentation algorithm for lung region identification in chest X-ray images [7]. This integration leverages the unsupervised nature of KM clustering, which uses the Euclidean distance between pixel intensities to form clusters, with the number of clusters fixed at 2. Comparative analysis against the Expectation Maximization with Gaussian Mixture Model (GMM-EM) showed that KM clustering, within the DE-PSO framework, yielded a marginally higher accuracy of 87.43%, as opposed to GMM-EM's 85.45%. This outcome highlights the effective application of KM clustering in the DE-PSO classifier, proving its capability to deliver precise segmentation in medical imaging.

Besides, previous researchers also implement KM clustering to segment out the lung regions from the CXR images based on the texture features extracted through the texture histogram and grey level co-occurrence matrix (GLCM) [8]. This research has segment 75 of COVID-19 negative and positive infected cases CXR images, while also achieving the accuracy of 92%.

Khatibi and Shahsavari [9] proposed a strategy to mitigate the disease burden by utilising CXR images for tuberculosis detection. The present study (CCNSE) introduces an innovative model for multi-instance classification that relies on Convolutional Neural Networks (CNNs), complex networks, and stacked ensembles. The performance metrics for the type of MC/SZ yielded an AUC of 99.000.28/98.000.16 and an accuracy of 99.260.40/99.220.32. The study utilised a fivefold cross-validation approach. The results indicate that the proposed method outperforms the alternative techniques in comparing tuberculosis diagnosis using chest X-ray images.

As an optimisation model for COVID-19 diagnosis, Anter and Oliva [10] developed a modified Slime Mould Algorithm (SMA) based on Levy distribution and adaptive Fuzzy C-means (AFCM). An SMA optimizer, which was used to build the best path for food connectivity, is provided. Weights will be adjusted in oscillation mode, simulating the propagation wave's process of producing both positive and negative feedback. In light of these findings, the accuracy of the suggested model is about (ACC = 0.96, RMSE = 0.23, Prec. = 0.98, F1 score = 0.98, MCC = 0.79, and Kappa = 0.79).

Ranjbarzadeh *et al.*, [11] have proposed a method for detecting and classifying COVID-19 infection from CT images utilising a two-route convolutional neural network (CNN) that extracts global and local properties. The proposed approach integrates fuzzy c-means clustering and regional directional pattern (LDN) encoding methodologies to represent the input image distinctly. The results indicate that the proposed framework achieved a precision rate of 96%, a recall rate of 97%, an F-score, an average surface distance (ASD) of 2:80:3 mm, and a volume overlap error (VOE) of 5:61:2%.

A fully automated segmentation method that can swiftly perform quantitative analysis of computed tomography images and is resistant to a number of density-enhancing lung problems has been proposed by Gerard *et al.*, [12]. The suggested lung segmentation technique was quantitatively assessed on 87 COVID-19 CT images using semi-automated and manually corrected segmentation. The outcomes showed a Dice coefficient of 0.985 mm and an average symmetric surface distance of 0.495 mm and 0.011 mm, respectively. The annotated dataset's accessibility is severely hampered by the fact that the disease is currently spreading at various rates throughout the world.

The segmented CXR image that was obtained will aid medical professionals in making accurate diagnoses. As a result, knowledge of the lung segments enables us to measure lung characteristics, such as size, that may be important for medical evaluation. The challenge of accurately segmenting lungs in chest X-rays arises from the presence of opacities or consolidation, which can result from overlaps between the lung region and severe abnormalities caused by pulmonary diseases, fluid, or bacterial infection [13]. Computer-aided diagnosis (CAD) systems are known to generate reliable segmentation outcomes owing to the distinct contrast observed between the lung region and its surrounding area in healthy individuals. In cases of pulmonary disease, the differentiation between the impacted lung region and the surrounding area on the film is often indistinct, leading to a decrease in the precision of segmentation. This is especially significant as accurate segmentation is imperative in such scenarios. Consequently, the undertaking of lung segmentation is significantly more difficult and complex.

Based on the summary of the previous works, there is a demand for detection and segmentation of lung region in CXR image as this step is important towards accurate diagnosis using computer-aided diagnostic systems (CADs). To resolve the challenges listed above, this study proposed a computerised approach to increase lung segmentation accuracy by utilizing Lazy Snapping algorithm as pre-segmentation step to automatically remove the bone of the chest area, followed by

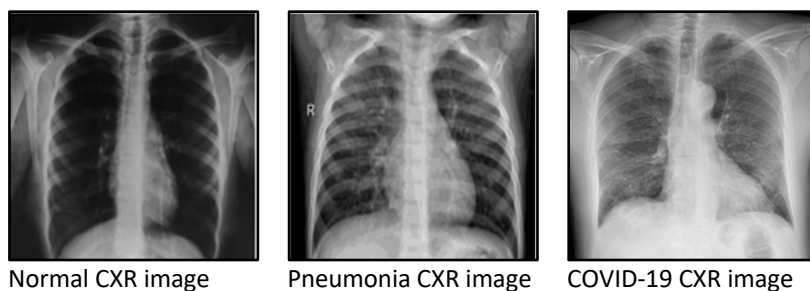
segmentation using clustering to accurately segment the desired lung area. To achieve and highlight the obtained result, the processes are summarized as follows:

- i. The raw CXR images utilized in this study were obtained from Covid19-Radiography and Chest-Xray-Images (Pneumonia) datasets.
- ii. The images were pre-segmented using Lazy Snapping to initially remove the bone of the chest area.
- iii. Modified global contrast stretching was employed to increase the significant contrast between the lung and the bone of chest region.
- iv. K-means and fast k-means clustering were used to accurately segment the desired lung area.
- v. To evaluate the performance, six metrics were computed: accuracy, sensitivity, specificity, precision, recall and F-score.

## 2. Methodology

### 2.1 Data Source and Description of Chest X-Ray Images

The Covid19-Radiography-Dataset and Chest-Xray-Images (Pneumonia) datasets, both of which are published in Kaggle, are two publicly accessible datasets and online sources that were used in this work. These datasets were selected because CXR images can reveal GGO patterns in the virus infected lung tissues, which is an important feature for medical imaging diagnosis. Typically, normal CXR images exhibit clear, darker areas representing the lung fields, whereas pneumonia shows the GGO patterns at the infected lung tissues only [14]. In contrast, COVID-19 often results in widespread GGO across the lungs, reflecting the virus's extensive impact [15]. The datasets include a variety of CXR image sizes. For this study, 150 CXR images were used, including 50 normal, 50 pneumonia, and 50 COVID-19 cases, to analyse the differences in lung appearances. These images serve as a representative sample for the investigation, with examples of normal, pneumonia, and COVID-19 CXR images illustrated in Figure 1.



**Fig. 1.** Samples of CXR images for normal, pneumonia and COVID-19 images

### 2.2 Image Pre-Processing and Segmentation of Chest X-Ray Images

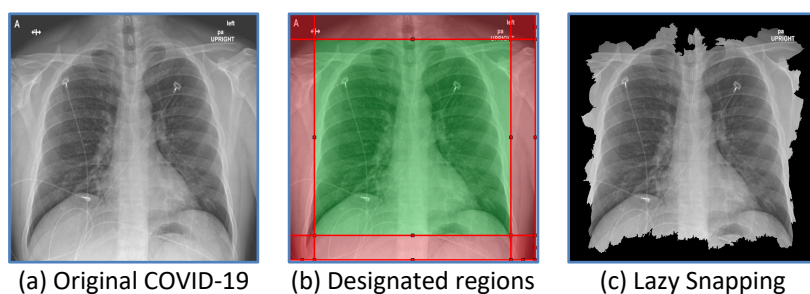
#### 2.2.1 Pre-segmentation of chest x-ray images using lazy snapping

A CXR image consists of a lung region which is referred as the region of interest, surrounded by the bone of chest regions (shoulder, scapula, diaphragm and thorax). For accurate learning and classification in the next processing stage, lung segmentation requires eliminating the surrounding areas from the chest radiograph. Increasing segmentation accuracy in medical imaging enables more accurate disease identification. By referring to the CXR images in Figure 1, it is noticeable that the

pixel values of the thoracic structure are similar to the soft tissues surrounded the lung region. Furthermore, the signs of the cloud region known on CXR imaging as Ground-Glass Opacity (GGO) are among the abnormalities that can be seen in the lungs for diagnosis the presents of COVID-19. Therefore, lung segmentation is crucial to obtain a good segmented image as the present of GGO might cause the under/over segmented images as the GGO area might be mistakenly segmented as part of thoracic structure. To overcome these shortcomings, lung region segmentation based on Lazy snapping algorithm has been proposed as pre-segmentation step to automatically remove the shoulder, scapula, diaphragm, and thorax regions from the CXR images.

Based on a graph cut, lazy snapping [16] employs interactively drawn lines to define which portions of the image should be maintained (referred to as the foreground) and which should be cut (referred to as the background). To minimise the Gibbs Energy  $E(X)$  on a graph concerning the user-defined hard restrictions, Graph Cut assigns labels to each node  $x_i$  (such as 1 for foreground and 0 for background). The isolated zones are calculated and presented for each new line that the user draws on the foreground and background areas of the image [17]. The user may properly crop the right area with just a few lines. Lazy Snapping employed the watershed approach as its initial step to pre-segment images. Next, a weighted directed graph was built by rendering the partitioned regions as nodes, and the graph partition problem was then solved using the maximum flow-minimum cut algorithm. Finally, to improve the segmentation results, a manual adjustment strategy is used.

The Lazy Snapping algorithm is comprehensively expounded in reference [16]. The requirement for interactive speeds in lung segmentation, especially when dealing with a high volume of images to be segmented, renders implementing a standard graph cut impractical. This is due to the user's need to select foreground and background regions for each input image manually. This study proposes an updated manual marking stage that utilises the location information of the lung on each input image to differentiate between the background and foreground regions, thereby overcoming the restriction above. Before analysing image data in this study, background and foreground regions were standardised to account for the varying proportions of the images used. Consequently, only the foreground portions could be automatically removed. Figure 2 displays a comparison between the original image and the image generated through the utilisation of the lazy snapping technique. From Figure 2(b), which depicts an appearance consisting of distinct regions, the foreground and background are automatically identified by the red and green frames, respectively.



(a) Original COVID-19 (b) Designated regions (c) Lazy Snapping  
**Fig. 2.** The designated regions and segmentation results of Lazy Snapping on CXR images

As mentioned earlier, lazy snapping algorithm utilized watershed algorithm as it first step to pre-segment images. As watershed uses the gradient information of grayscale images, this may result on over-segmentation image, in where the number of regions of the pre-segmentation results is still large. Therefore, the resultant segmented image needs to under two additional steps, which are contrast stretching and clustering to improve the segmentation performance of the detection lung region.

### 2.2.2 Image enhancement by using modified global contrast stretching technique

The chest radiograph images captured from the radiography device could have various flaws, including blurriness or low contrast, hence requires an enhancement process. This is typically done to highlight image details that may be difficult for a human viewer to recognize. Generally, image enhancement aims to enhance the diminishing features of the image, thus improving the image quality to be used for training the model. However, the purpose of using image enhancement is slightly different for this study, where it is used to increase the significant contrast between the lung and the bone of chest regions for easing the segmentation process.

Thus, a contrast enhancement technique namely modified global contrast stretching (MGCS) [18] is utilized to improve the image quality and increase the contrast of CXR image. Contrast stretching is known to enhance the image by widening the range of scene illumination. This technique attempts to improve the contrast in an image by extending the image's intensity values to cover a desired range of values, usually the entire range of pixel values permitted by the image type. As for MGCS, the updated stretching methods for the modified version are analogous to the minimum-maximum values of the conventional global and linear contrast stretching [19]. The CXR image will be improved by performing the MGCS approach with 25% as the minimum percentage, *minp*, and 25% as the maximum percentage, *maxp*, values. By using these settings, the pixel within the range of *minp* and *maxp* will be mapped and stretched to a wider range, while the remaining pixels will be compressed. Thus, the bone of chest area becomes brighter, while the lung area becomes darker, hence the contrast between these two regions is raised while simultaneously simplifying the image segmentation process.

### 2.2.3 Lung segmentation using variant K-means based clustering techniques

Once the CXR image was enhanced, the lung segmentation process was repeated using a clustering approach. For this purpose, an adaptive unsupervised segmentation technique based on k-means and fast k-means clustering algorithms will be utilized for easily segmenting the lung region.

K-Means (KM) Clustering [20]: is one of the most commonly used unsupervised learning algorithms due to its straightforwardness and computational efficiency. It is particularly effective for large datasets, making it suitable for medical imaging analysis, including lung segmentation. K-means divides an unlabelled data set into K clusters, where each level value should be assigned to the cluster with the closest cluster centre after calculating the Euclidean distance between each level value and the cluster's centre. The clusters were constructed using its similarity. In order to analyse the number of clusters towards lung segmentation, different number of clusters have been analysed consisting of K=2, 4, 6, 8 and 10. The aim of k-means clustering is to minimized the objective function as shown in Eq. (1):

$$J = \sum_{i=1}^n \sum_{j=1}^k \|x_i - c_j\|^2 \quad (1)$$

When  $x_i$  is the  $i$ -th sample,  $k$  is the number of clusters,  $n$  is the quantity of data, and  $c_j$  is the  $j$ -th cluster center. Each element of data in this study will be divided into three groups for all analyses. The KM clustering algorithm for image segmentation can be implemented as follows:

- i. The clustering of the pixels is done by choosing k points at random from the space. The initial cluster centre,  $c_j$ , is represented by these points.
- ii. Each data should be given to the closest centre.
- iii. Recalculate the new centre location once all the data have been assigned.
- iv. Once the centres are no longer moving, repeat steps 2 and 3 once again. As a result, the item will be divided into groups from which the metric that needs to be minimized can be calculated.

Fast K-Means (FKM) Clustering [21]: Lung segmentation is a crucial step since it isolates the objects of interest which is referred to the lung region for later processing or recognition steps. Since CXR images are downloaded from the internet, object elements with different intensities may result in lighter and darker regions, which may compromise the precision of conventional image segmentation. Therefore, FKM clustering is preferable as compared to the conventional KM as it offers more benefits in terms of segmentation performance as well as its timing [21,22]. FKM clustering can minimize the time required to train image cluster centres and solve the problem of retraining cluster centres. The following is a precise explanation of the FKM clustering steps:

- i. The histogram discrete function value is  $h(rR,i1, rG,i2, rB,i3)$  where  $i1, i2, i3 = 1, 2, \dots, L$  or call all the pixels to have colour level  $rR,i1, rG,i2, rB,i3$ . This assumes that an RGB image database (R, G, and B) comprises N images and the j-th.
- ii. If there are K clusters and n centre vectors per cluster, then:

$$c_k = (c_{k,1}, \dots, c_{k,n}) \quad (2)$$

where  $k = 1, 2, \dots, K$ .

- iii. Determine the closest cluster centre by calculating the Euclidean distance between each level value and it. The k-th cluster vector's level value r and cluster centre  $c_k$  are separated by the following Euclidean distance:

$$d(r, c_k) = \sqrt{(r_1 - c_{k,1})^2 + \dots + (r_n - c_{k,n})^2} \quad (3)$$

where  $k = 1, 2, \dots, k$ . The cluster  $c_k$  of its nearest cluster centre is given the colour scale value r.

- iv. By calculating the mean of each cluster level, create a new centre for each cluster.
- v. Until the new cluster centre is equal to the starting database, repeat steps 1 through 3.

The image chosen for FKM has single colour components. Thus, the histogram discrete function value will be  $h(r_{i1}, r_{i2}, r_{i3} \dots r_{in})$  until all of the pixels in the image are analysed. Because the value of 'k' is set to 2, the images will only be segmented into two clusters. Let's K value is set to 2, then the precise of two centre points will be constructed. The processes will be repeated to determine the precise two centre spots. The Euclidean distance between each level value and the cluster centre  $C_k$  is then calculated. Following that, each level value will be sorted and clustered to the cluster centre point that is nearest to it. The new centre point will be determined using the mean value. Then, all noises and unwanted images are removed to make sure the image of the lungs is white, with a black background and no visible bone shape.

#### *2.2.4 Image post-processing for chest x-ray images*

The segmented image produced from the previous step may consist of some unwanted objects attached to the border of the segmented image. Hence, the unwanted objects were discarded by removing all objects that are less than 50,000 pixels in size. Finally, the surface of the segmented lung region and its boundary were smoothed by using a disk-shaped structure element with a radius of 25 pixels in close morphology.

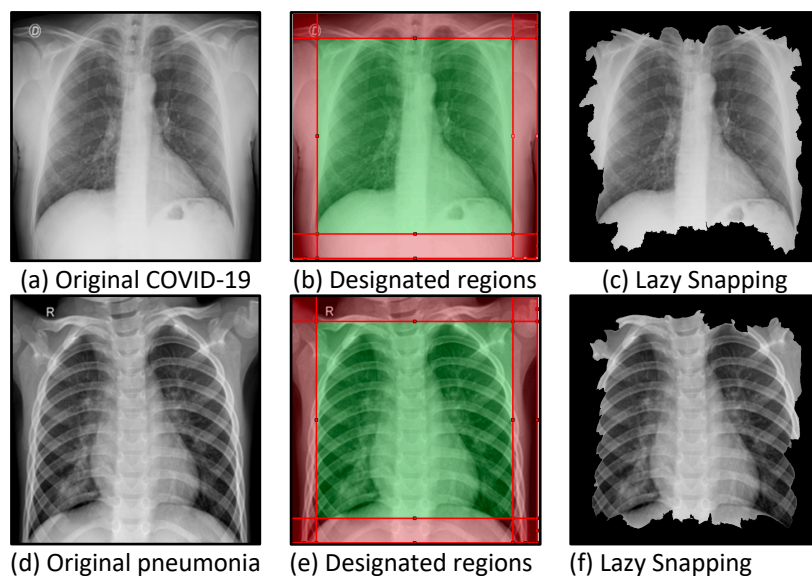
### **3. Results and Discussions**

In this study, lung region segmentation that can automatically remove the bone of the chest area by utilizing Lazy Snapping and clustering segmentation approaches has been proposed. Comparisons between two approaches by applying multi-level segmentation (Lazy Snapping and clustering) and single segmentation (clustering only) were conducted to recognize the significance of applying each segmentation approach on CXR images. To assess the impact of lung segmentation, the major criterion for evaluating the performance of each segmentation strategy is based on its capacity to produce fully segmented lung areas as well as remove the bone of chest regions from the image. Both qualitative and quantitative criteria have been used to evaluate the characteristics of segmented images.

In this study, the experiment was performed on 150 CXR images of COVID-19, pneumonia, and normal samples. Figure 3 shows a sample of CXR images, and the results obtained by employing Lazy Snapping. In this study, the CXR image was pre-segmented by using Lazy Snapping to initially remove the bone of chest regions from the image. This algorithm was used as an additional step to improve the segmentation performance of the detected lung region. To perform the pre-segmentation, each image was marked by specifying the lung and background regions depending on the position information of the lung on each input image. The position of these designated regions was standardized and suitable to be applied for all 150 images.

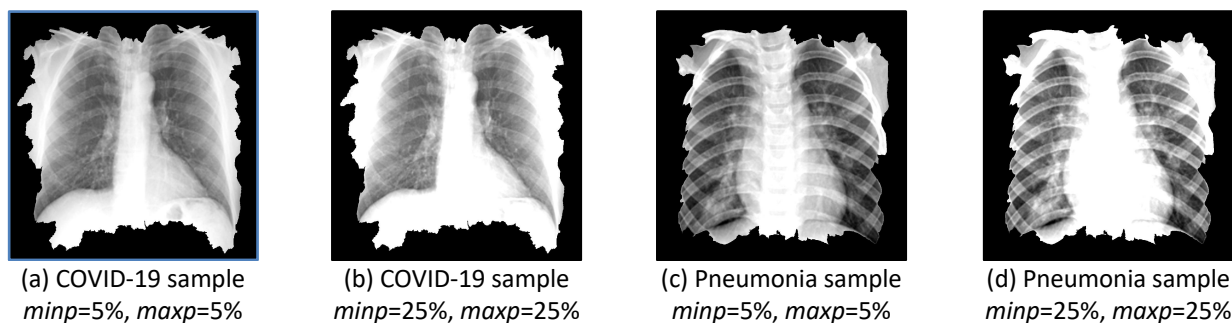
Figure 3 represents the designated regions, where the red frame marks lung information, while the green frame marks the background. The lung field was recovered from the image after removing the shoulder and diaphragm regions based on the outcomes of Lazy Snapping. Hence, Lazy Snapping proved to be an efficient and reliable approach that could be used as pre-segmentation for removing a larger part of the bone region in the image. Nevertheless, it was noted that this particular methodology exhibits a bias towards over-segmentation, given that the thoracic region persists in the foreground, and the left and right lungs are predominantly not differentiated. The need for more specification of the thoracic vertebra as contextual information during implementation of the Lazy Snapping methodology resulted in the above outcome. Thus, a complex structural area like this could be addressed by segmenting the result a second time using a clustering approach.





**Fig. 3.** The designated regions and segmentation results of Lazy Snapping on CXR images.

To correct the condition caused by over-segmentation, the resulting image was further enhanced using MGCS technique. This step is necessary to increase the significant contrast between the lung and the bone of chest regions for easing the segmentation process. Figure 4 presents a sample of CXR image from COVID-19 patient that has undergone the MGCS process. By applying the contrast stretching with high and constant values of  $minp=25\%$  and  $maxp=25\%$ , the bone of chest area becomes brighter, while the lung area becomes darker, hence increasing the contrast between these two regions. If the maximum value is higher than the minimum value, the bone area will appear brighter. If the lowest value is higher than the highest value, the lung region will seem darker. This enhancement step partially eliminates the intensity variations between the lung and its background.


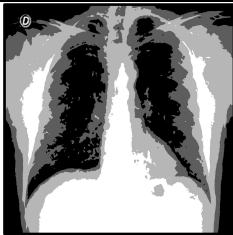
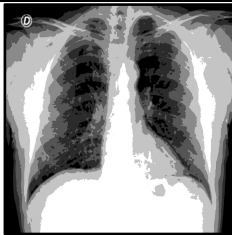
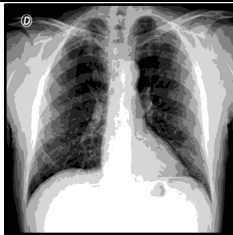
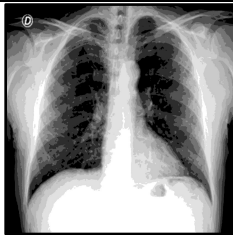

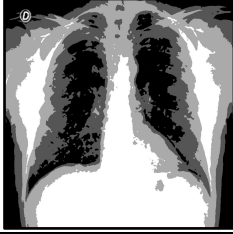
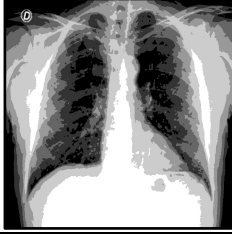
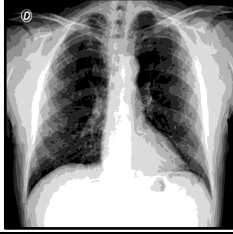
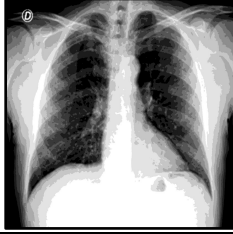


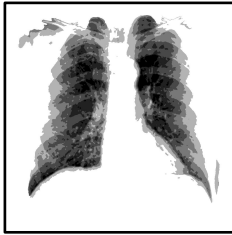



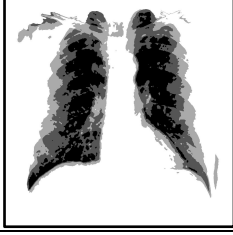





**Fig. 4.** Contrast enhancement based on MGCS applied to a CXR from a patient with COVID-19

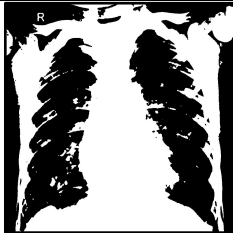
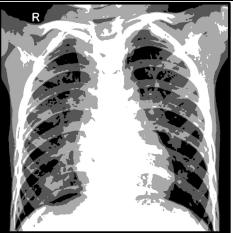
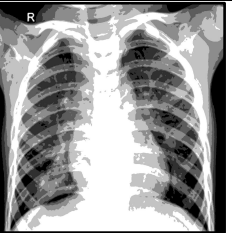
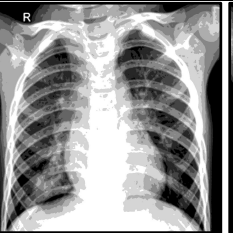
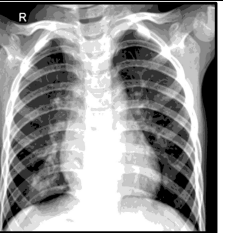
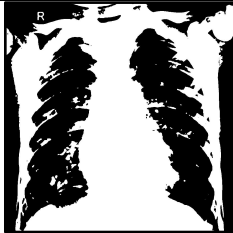
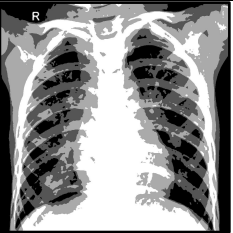
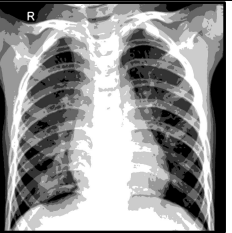
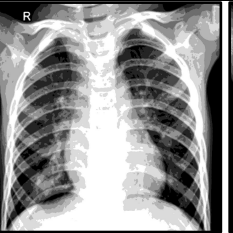
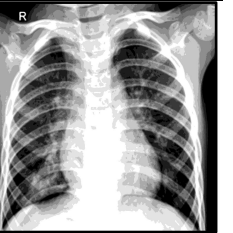
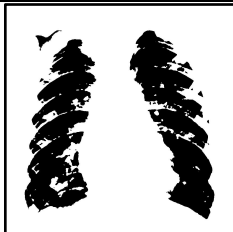
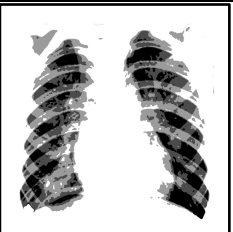
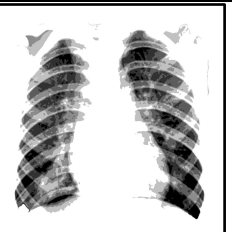
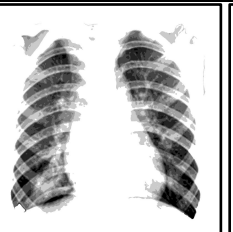
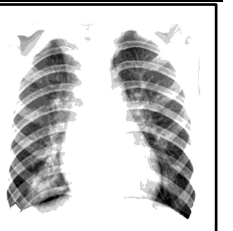
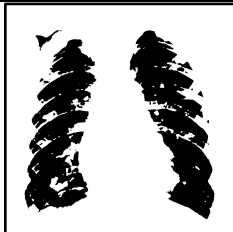
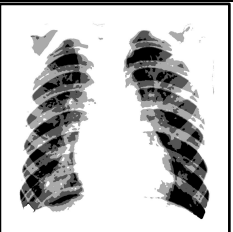
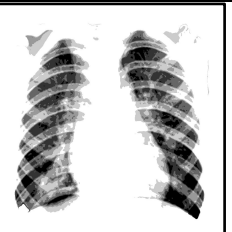
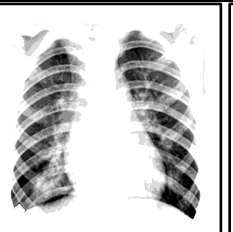
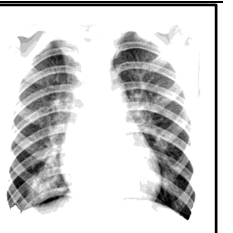
Thereafter, a segmentation procedure employing KM and FKM clustering algorithms was carried out to obtain a finer viewpoint for the region of interest, which is the lung area as presented in Table 1 and Table 2. To examine the importance of each clustering approach for image segmentation, segmentation has been performed using various numbers of clusters (segmented regions). Table 3 and Table 4 illustrate the final results of the proposed segmentation approach. As mentioned earlier, there are two different experiments (combination of Lazy Snapping and clustering versus clustering only) were conducted for recognizing the significance of applying each segmentation approaches on CXR image. By referring to the final results of single segmentation, KM is unable to segment the lung region properly when using number of clusters of 4, as the left side of the lung region disappears after the image segmentation phase is complete. By observing the results of KM clustering, the

segmented regions produced by the five set of clusters vary as the number of clusters varies. Furthermore, under-segmented lung region has been produced when applying number of clusters equal to 4, 6 and 8. Thus, choosing the right number of clusters is essential for appropriately segmenting the lung region with KM clustering.

**Table 1**  
 Results of lung segmentation of COVID-19 sample after applying KM and FKM clustering algorithms





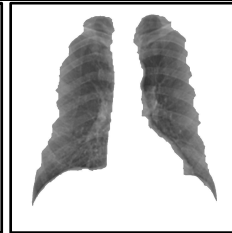
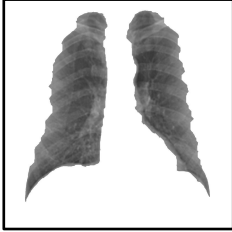
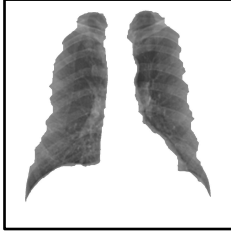

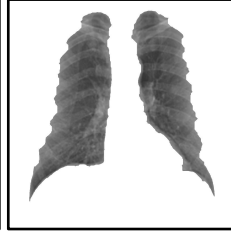
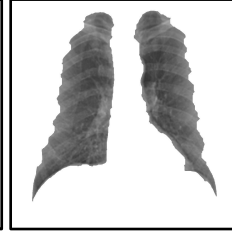
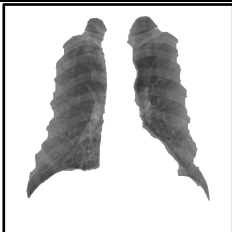
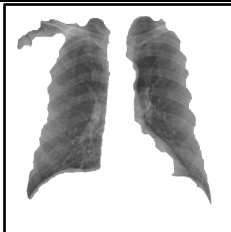
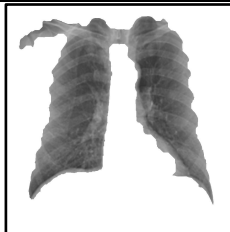
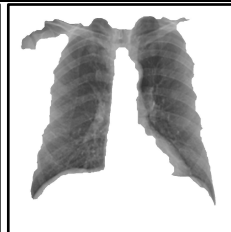
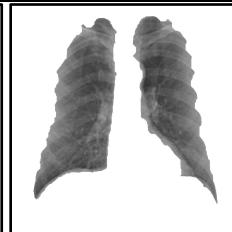

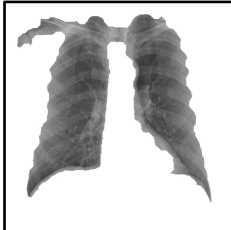


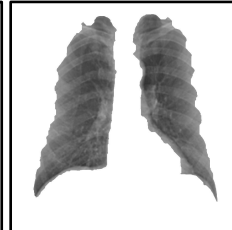
	2 clusters, read 1 region	4 clusters, read 2 regions	6 clusters, read 3 regions	8 clusters, read 4 regions	10 clusters, read 5 regions
KM					
FKM					
	2 clusters, read 1 region	4 clusters, read 3 regions	6 clusters, read 5 regions	8 clusters, read 7 regions	10 clusters, read 9 regions
Lazy Snapping + KM					
Lazy Snapping + FKM					

**Table 2**  
 Results of lung segmentation of pneumonia sample after applying KM and FKM clustering algorithms

	2 clusters, read 1 region	4 clusters, read 2 regions	6 clusters, read 3 regions	8 clusters, read 4 regions	10 clusters, read 5 regions
KM					
FKM					
	2 clusters, read 1 region	4 clusters, read 3 regions	6 clusters, read 5 regions	8 clusters, read 7 regions	10 clusters, read 9 regions
Lazy Snapping + KM					
Lazy Snapping + FKM					

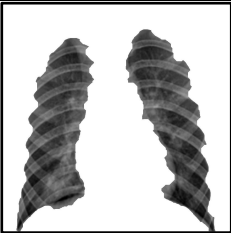
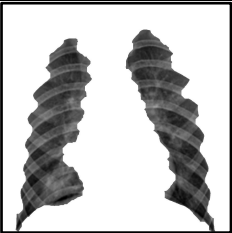
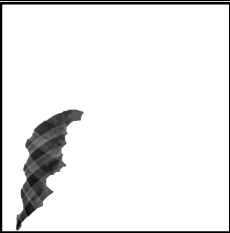

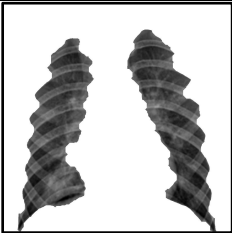
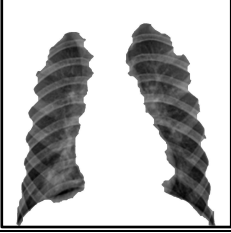
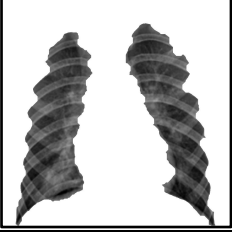
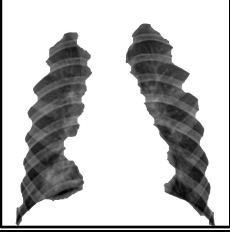
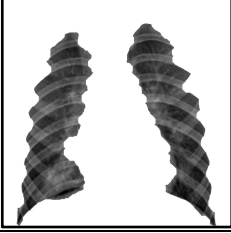
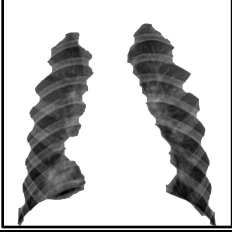

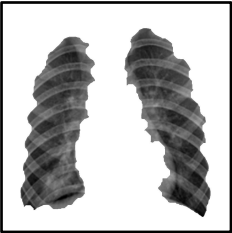
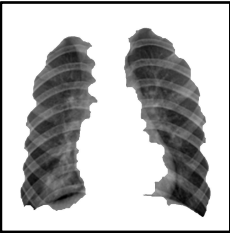
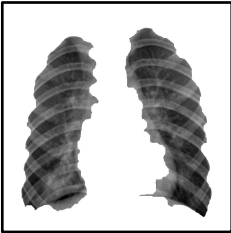
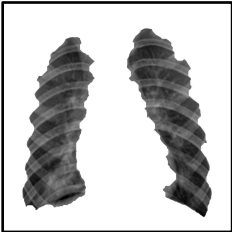
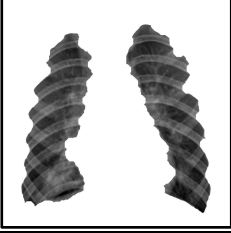
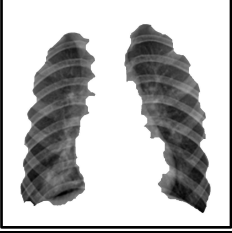


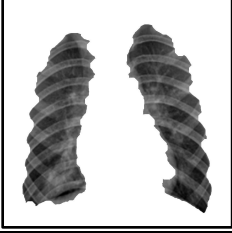
Interestingly for FKM, as the number of clusters increase to 10, each set of clusters has produced homogeneous results and the segmented lung region are better compared to KM. Most of the areas on the border of the lung that contain GGO feature for COVID-19 sample are still available for FKM image. However, in terms of single image segmentation approach, it was also observed that using KM and FKM alone have led to under-segmentation tendency in processing the image as this clustering are sensitive to intensity variations of the input image. However, in case of complex CXR images segmentation problems, which cannot be tackled effectively by using clustering segmentation alone, applying multi-level segmentation is the most suitable approach. After performing clustering on a segmented Lazy Snapping image, the left and right lungs could be separated. It is evident from Table 3 and Table 4 that the proposed combination of Lazy Snapping and clustering approach achieves very promising segmentation results in most of the images, under the same position of this designated regions, as well as variety number of clusters, which is more effective in practical applications.

**Table 3**  
 Results of segmented lung of COVID-19 sample after post-processing

	2 clusters, read 1 region	4 clusters, read 2 regions	6 clusters, read 3 regions	8 clusters, read 4 regions	10 clusters, read 5 regions
KM					
FKM					
	2 clusters, read 1 region	4 clusters, read 3 regions	6 clusters, read 5 regions	8 clusters, read 7 regions	10 clusters, read 9 regions
Lazy Snapping + KM					
Lazy Snapping + FKM					

To further compare and evaluate the segmentation quality of each segmentation approach, the statistical values of the segmented CXR images are compared with the ground truth images by picking sensitivity, specificity, accuracy, precision, recall and f-score. Using 3D-Paint, each CXR image was manually segmented to produce the ground truth images. The comparison was made using 150 CXR images, with 50 images each for COVID-19, pneumonia, and normal samples. The segmentation performance has been reported for the different clustering approaches in Table 5. Given that the goal of the segmentation is to precisely separate the targeted lung region from the chest bone region, it can be seen that FKM in a combination with Lazy Snapping as the pre-segmentation step outperformed the others with accuracy and F-score of 92.38% and 0.8739, respectively.

**Table 4**  
 Results of segmented lung of pneumonia sample after post-processing

	2 clusters, read 1 region	4 clusters, read 2 regions	6 clusters, read 3 regions	8 clusters, read 4 regions	10 clusters, read 5 regions
KM					
FKM					
	2 clusters, read 1 region	4 clusters, read 3 regions	6 clusters, read 5 regions	8 clusters, read 7 regions	10 clusters, read 9 regions
Lazy Snapping + KM					
Lazy Snapping + FKM					

It was further verified in Table 5 that Lazy Snapping has consistently improved the segmentation performance for both KM and FKM clustering. Furthermore, single segmentation based on KM clustering was worst-performing with accuracy and F-score of 83.72% and 0.7653. Additionally, it can be seen that, when compared to KM, the FKM is the clustering technique that performs the best for both single and multi-level segmentation. Overall, it is clear that the combination of Lazy Snapping and clustering was the best-performing technique, both in terms of high sensitivity values that surpassed the solo clustering and accuracy of segmentation performance. Therefore, the results of the proposed segmentation approach reported in this study are proved to be efficient and hence, a reliable approach that could be used in lung region segmentation for aiding COVID-19 diagnosis.

**Table 5**

Differences of clustering techniques, the result of average segmentation performance of two different segmentation techniques

Clustering Method	Number of Clusters	Sensitivity (%)	Specificity (%)	Accuracy (%)	Precision	Recall	F-score
K-Means	2 Cluster	58.09	98.38	86.04	0.9449	0.5809	0.7868
	4 Cluster	55.73	98.54	85.34	0.9483	0.5573	0.7599
	6 Cluster	49.86	98.85	83.72	0.9565	0.4986	0.7653
	8 Cluster	54.39	98.57	85.00	0.9481	0.5439	0.7706
	10 Cluster	53.43	98.78	84.81	0.9537	0.5343	0.7703
Fast K-Means	2 Cluster	59.09	98.33	86.36	0.9440	0.5909	0.7790
	4 Cluster	59.53	98.50	86.43	0.9493	0.5953	0.7640
	6 Cluster	62.58	98.50	87.37	0.9528	0.6258	0.7575
	8 Cluster	59.13	98.57	86.39	0.9524	0.5913	0.7538
	10 Cluster	57.88	98.61	86.07	0.9525	0.5788	0.7597
Lazy Snapping + KM	2 Cluster	77.24	98.36	91.36	0.9525	0.7724	0.8479
	4 Cluster	87.66	94.27	91.76	0.8708	0.8766	0.8665
	6 Cluster	76.78	98.02	91.02	0.9456	0.7678	0.8427
	8 Cluster	85.46	94.91	91.59	0.8848	0.8546	0.8609
	10 Cluster	84.90	95.86	92.04	0.9026	0.8490	0.8671
Lazy Snapping + FKM	2 Cluster	77.45	98.34	91.42	0.9521	0.7745	0.8490
	4 Cluster	88.08	94.01	91.72	0.8665	0.8808	0.8665
	6 Cluster	78.56	98.05	91.48	0.9450	0.7856	0.8523
	8 Cluster	83.05	97.04	92.21	0.9241	0.8305	0.8693
	10 Cluster	85.23	96.27	92.38	0.9088	0.8523	0.8739

#### 4. Conclusion

In this study, a multi-level image segmentation method based on Lazy Snapping and clustering is proposed. The proposed methodology employs the Lazy Snapping algorithm as a pre-segmentation technique to facilitate the automated removal of the bone from the chest region. Subsequently, segmented clustering is employed as nodes to delineate the requisite lung area. By employing this strategy, a better lung segmentation result has been achieved using multi-level segmentation approach as compared of using a single clustering algorithm for image segmentation. The experimental results show that the proposed approach can achieve segmentation with the accurate desired region while retaining the important boundary details and shows good performance in most evaluation indexes. From the results of numerical experiments, the performances of multi-level segmentation using FKM is found to be slightly effective than the KM algorithm with average segmentation accuracy and f-score values of 92.38% and 0.8739, respectively.

Future research directions will focus on advancing image classification techniques to diagnose the COVID-19 disease automatically. Leveraging the groundwork laid by successful multi-level segmentation, the next step would be exploring the integration of sophisticated image classification algorithms, such as CNN and support vector machine (SVM), to refine the detection and analysis of COVID-19 and other pulmonary conditions. An area of particular interest is the cross-modal analysis, where segmented X-ray imagery will be synergized with clinical data, augmenting the predictive capacity of classification models. This diagnostic tool not only facilitates fast and accurate disease diagnose but also supports tailored treatment strategies, marking a significant leap forward in the domain of lung disease diagnostics.

## Acknowledgement

The author would like to acknowledge the support from the Fundamental Research Grant Scheme (FRGS) under a grant number of FRGS/1/2021/TK0/UNIMAP/02/37 from the Ministry of Higher Education Malaysia.

## References

- [1] Goyal, Shimpy, and Rajiv Singh. "Detection and classification of lung diseases for pneumonia and Covid-19 using machine and deep learning techniques." *Journal of Ambient Intelligence and Humanized Computing* 14, no. 4 (2023): 3239-3259. <https://doi.org/10.1007/s12652-021-03464-7>
- [2] Malik, Hassaan, Tayyaba Anees, Muizzud Din, and Ahmad Naeem. "CDC\_Net: Multi-classification convolutional neural network model for detection of COVID-19, pneumothorax, pneumonia, lung Cancer, and tuberculosis using chest X-rays." *Multimedia Tools and Applications* 82, no. 9 (2023): 13855-13880. <https://doi.org/10.1007/s11042-022-13843-7>
- [3] Sanghvi, Harshal A., Riki H. Patel, Ankur Agarwal, Shailesh Gupta, Vivek Sawhney, and Abhijit S. Pandya. "A deep learning approach for classification of COVID and pneumonia using DenseNet-201." *International Journal of Imaging Systems and Technology* 33, no. 1 (2023): 18-38. <https://doi.org/10.1002/ima.22812>
- [4] Almotairi, Khaled H., Ahmad MohdAziz Hussein, Laith Abualigah, Sohaib KM Abujayyab, Emad Hamdi Mahmoud, Bassam Omar Ghanem, and Amir H. Gandomi. "Impact of artificial intelligence on COVID-19 pandemic: a survey of image processing, tracking of disease, prediction of outcomes, and computational medicine." *Big Data and Cognitive Computing* 7, no. 1 (2023): 11. <https://doi.org/10.3390/bdcc7010011>
- [5] Xue, Xingsi, Seelammal Chinnaperumal, Ghaida Muttashar Abdulsahib, Rajasekhar Reddy Manyam, Raja Marappan, Sekar Kidambi Raju, and Osamah Ibrahim Khalaf. "Design and analysis of a deep learning ensemble framework model for the detection of COVID-19 and pneumonia using large-scale CT scan and X-ray image datasets." *Bioengineering* 10, no. 3 (2023): 363. <https://doi.org/10.3390/bioengineering10030363>
- [6] Abd Elaziz, Mohamed, Mohammed AA Al-Qaness, Esraa Osama Abo Zaid, Songfeng Lu, Rehab Ali Ibrahim, and Ahmed A. Ewees. "Automatic clustering method to segment COVID-19 CT images." *PLoS One* 16, no. 1 (2021): e0244416. <https://doi.org/10.1371/journal.pone.0244416>
- [7] Dixit, Abhishek, Ashish Mani, and Rohit Bansal. "CoV2-Detect-Net: Design of COVID-19 prediction model based on hybrid DE-PSO with SVM using chest X-ray images." *Information sciences* 571 (2021): 676-692. <https://doi.org/10.1016/j.ins.2021.03.062>
- [8] Sumarti, Heni, Qolby Sabrina, Devi Triana, Fahira Septiani, and Tara Puri Ducha Rahmani. "Identification of Covid-19 based on features texture histogram and gray level co-occurrence matrix (glcm) using k-means clustering methods in chest X-ray digital images." *Jurnal Penelitian Fisika dan Aplikasinya (JPFA)* 13, no. 1 (2023): 51-66. <https://doi.org/10.26740/jpfa.v13n1.p51-66>
- [9] Khatibi, Toktam, Ali Shahsavari, and Ali Farahani. "Proposing a novel multi-instance learning model for tuberculosis recognition from chest X-ray images based on CNNs, complex networks and stacked ensemble." *Physical and Engineering Sciences in Medicine* 44, no. 1 (2021): 291-311. <https://doi.org/10.1007/s13246-021-00980-w>
- [10] Anter, Ahmed M., Diego Oliva, Anuradha Thakare, and Zhiguo Zhang. "AFCM-LSMA: New intelligent model based on Lévy slime mould algorithm and adaptive fuzzy C-means for identification of COVID-19 infection from chest X-ray images." *Advanced Engineering Informatics* 49 (2021): 101317. <https://doi.org/10.1016/j.aei.2021.101317>
- [11] Shan, Fei, Yaozong Gao, Jun Wang, Weiya Shi, Nannan Shi, Miaofei Han, Zhong Xue, Dinggang Shen, and Yuxin Shi. "Lung infection quantification of COVID-19 in CT images with deep learning." *arXiv preprint arXiv:2003.04655* (2020).
- [12] Gerard, Sarah E., Jacob Herrmann, Yi Xin, Kevin T. Martin, Emanuele Rezoagli, Davide Ippolito, Giacomo Bellani *et al.*, "CT image segmentation for inflamed and fibrotic lungs using a multi-resolution convolutional neural network." *Scientific reports* 11, no. 1 (2021): 1455. <https://doi.org/10.1038/s41598-020-80936-4>
- [13] Rahman, Md Fashiar, Yan Zhuang, Tzu-Liang Bill Tseng, Michael Pokojovy, Peter McCaffrey, Eric Walser, Scott Moen, and Alex Vo. "Improving lung region segmentation accuracy in chest X-ray images using a two-model deep learning ensemble approach." *Journal of Visual Communication and Image Representation* 85 (2022): 103521. <https://doi.org/10.1016/j.jvcir.2022.103521>
- [14] Wang, Tianmu, Zhenguo Nie, Ruijing Wang, Qingfeng Xu, Hongshi Huang, Handing Xu, Fugui Xie, and Xin-Jun Liu. "PneuNet: deep learning for COVID-19 pneumonia diagnosis on chest X-ray image analysis using Vision Transformer." *Medical & Biological Engineering & Computing* 61, no. 6 (2023): 1395-1408. <https://doi.org/10.1007/s11517-022-02746-2>

- [15] Flor, Nicola, Stefano Fusco, Ivana Blazic, Marcelo Sanchez, and Ella Annabelle Kazerooni. "Interpretation of chest radiography in patients with known or suspected SARS-CoV-2 infection: what we learnt from comparison with computed tomography." *Emergency Radiology* 30, no. 3 (2023): 363-376. <https://doi.org/10.1007/s10140-022-02105-6>
- [16] Li, Yin, Jian Sun, Chi-Keung Tang, and Heung-Yeung Shum. "Lazy snapping." *ACM Transactions on Graphics (ToG)* 23, no. 3 (2004): 303-308. <https://doi.org/10.1145/1015706.1015719>
- [17] Shan, Yilin, Yan Ma, Yuan Liao, Hui Huang, and Bin Wang. "Interactive image segmentation based on multi-layer random forest classifiers." *Multimedia Tools and Applications* 82, no. 15 (2023): 22469-22495. <https://doi.org/10.1007/s11042-022-14199-8>
- [18] Abdul-Nasir, Aimi Salihah, Mohd Yusoff Mashor, and Zeehaida Mohamed. "Modified global and modified linear contrast stretching algorithms: New colour contrast enhancement techniques for microscopic analysis of malaria slide images." *Computational and mathematical methods in medicine* 2012 (2012). <https://doi.org/10.1155/2012/637360>
- [19] Nasir, A. S. A., N. A. A. Khairudin, L. C. Chin, T. A. Aris, and Z. Mohamed. "Enhanced  $k$ -Means Clustering Algorithm for Detection of Human Intestinal Parasites." In *2020 IEEE-EMBS Conference on Biomedical Engineering and Sciences (IECBES)*, pp. 372-377. IEEE, 2021. <https://doi.org/10.1109/IECBES48179.2021.9398801>
- [20] MacQueen, James. "Some methods for classification and analysis of multivariate observations." In *Proceedings of the fifth Berkeley symposium on mathematical statistics and probability*, vol. 1, no. 14, pp. 281-297. 1967.
- [21] Lin, Chuen-Horng, Chun-Chieh Chen, Hsin-Lun Lee, and Jan-Ray Liao. "Fast K-means algorithm based on a level histogram for image retrieval." *Expert Systems with Applications* 41, no. 7 (2014): 3276-3283. <https://doi.org/10.1016/j.eswa.2013.11.017>
- [22] Aris, Thaqifah Ahmad, Aimi Salihah Abdul Nasir, and Zeehaida Mohamed. "A robust segmentation of malaria parasites detection using fast k-means and enhanced k-means clustering algorithms." In *2021 IEEE International Conference on Signal and Image Processing Applications (ICSIPA)*, pp. 128-133. IEEE, 2021. <https://doi.org/10.1109/ICSIPA52582.2021.9576799>